Photoinduced Electron Transfer Pathways in Hydrogen-Evolving Reduced Graphene Oxide-Boosted Hybrid Nano-Bio Catalyst

Peng Wang,[†] Nada M. Dimitrijevic,[‡] Angela Y. Chang,[§] Richard D. Schaller,[†,§] Yuzi Liu,[†] Tijana Rajh,[†] and Elena A. Rozhkova[†,*]

[†]Center for Nanoscale Materials and [‡]Chemical Sciences and Engineering Division, Argonne National Laboratory, Argonne, Illinois 60439, United States and [§]Department of Chemistry, Northwestern University, Evanston, Illinois 60208, United States

ABSTRACT Photocatalytic production of clean hydrogen fuels using water and sunlight has attracted remarkable attention due to the increasing global energy demand. Natural and synthetic dyes can be utilized to sensitize semiconductors for solar energy transformation using visible light. In this study, reduced graphene oxide (rGO) and a membrane protein bacteriorhodopsin (bR) were employed as building modules to harness visible light by a Pt/TiO_2 nanocatalyst. Introduction of the rGO boosts the nano-bio catalyst performance that results in hydrogen production rates of approximately 11.24 mmol of H_2 (μmol protein)$^{-1}$ h^{-1}. Photoelectrochemical measurements show a 9-fold increase in photocurrent density when TiO_2 electrodes were modified with rGO and bR. Electron paramagnetic resonance and transient absorption spectroscopy demonstrate an interfacial charge transfer from the photoexcited rGO to the semiconductor under visible light.

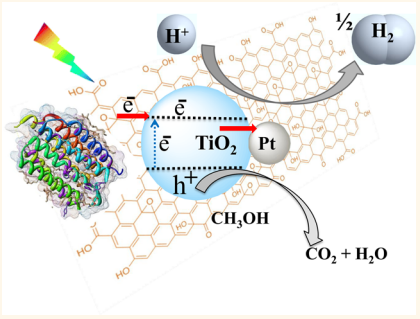

KEYWORDS: graphene · bacteriorhodopsin · Pt/TiO_2 nanoparticles · visible light · hydrogen fuels · nano-bio materials

Exploration of renewable and ecologically benign energy sources is one of the greatest challenges that may be able to address the escalating global energy demand. Sunlight energy transformation offers strategies to achieve the goals of clean energy for the near future.[1−3] Solar energy can be converted into chemical energy stored in the form of hydrogen or other chemical compounds.[4,5] Since the first report on photocatalytic splitting of water into oxygen and hydrogen on TiO_2 photoelectrodes under UV light by Fujishima and Honda,[6] there has been a great interest in developing visible-light-responsive photocatalysts because UV light accounts for only 4% of solar photons. Various methods of extending the visible light reactivity of TiO_2 including doping and sensitization by organic dyes or quantum dots[7−10] have been developed. One attractive approach for photocatalytic hydrogen production utilizes biological structures. Successful examples include photosynthetic complex,[11,12] metalloenzymes[13−16] or their cofactors,[17] light-harvesting accessory pigment complex,[18] and even raw biomass.[19] Recently, our group reported on the successful use of the photosensitive proton pump bacteriorhodopsin (bR) from halophilic (salt-loving) Archaea organisms assembled on a Pt/TiO_2 nanocatalyst as a robust biomaterial for visible-light-driven hydrogen generation.[20] The $bR/Pt/TiO_2$ hybrid nano-bio catalyst produces 5275 μmol of H_2 (μmol protein)$^{-1}$ h^{-1} at pH 7 in the presence of sacrificial substrates under ambient conditions.[20] El-Sayed's group also used bR as a building block to construct a bR/TiO_2 nanotube array hybrid electrode system with a 50% photocurrent density increase over that measured for pure TiO_2 nanotubes.[21] Compared to organic and inorganic photosynthesizers, bR is an integral transmembrane protein complex that contains a retinal photoreceptor prosthetic group and absorbs green light (absorption max at 568 nm). Archaea utilizes the membrane bR proton pump, also known as a purple membrane PM, as a biological solar cell to transform sunlight energy into a

* Address correspondence to rozhkova@anl.gov.

Received for review April 10, 2014 and accepted July 22, 2014.

Published online July 22, 2014
10.1021/nn502011p

transmembrane proton gradient and then for powering ATP synthesis *via* a mechanism evolutionary independent from chlorophyll-based photosynthesis. Being expressed by an extremophile, PMs are naturally evolved to tolerate, thrive, and maintain their photoreactivity under demanding conditions, including exposure to light and oxygen, high ionic strength (3 M NaCl), temperatures over 80 °C (in water) and 140 °C (dry), at pH values of 0−12 and digestion by proteases.[22] When bR is utilized as a functional module in a nano-bio photocatalyst, it assists in harnessing visible light. Besides, bR provides its biological functionality of the light-driven pumping of protons toward the hydrogen-evolving platinum cocatalyst, enabling enhanced evolution of hydrogen.[20,21]

Recently, several groups reported the successful incorporation of graphene as a component of composite materials for advancing the photocatalytic performance of semiconductors in water splitting and pollutant degradation that was summarized in excellent topical reviews.[23−26] Graphene, a single layer of sp^2-bonded carbon atoms arranged in a two-dimensional honeycomb lattice, possesses excellent mechanical, thermal, and optical characteristics, high conductivity, and electron mobility properties and provides large specific surface area.[27−29] Hydrophilic graphene oxide (GO) and reduced graphene oxide (rGO) could be considered as graphene functionalized with oxygen-centered groups such as carboxylic, hydroxyl, or epoxide that allows for interaction with positively charged molecules and can serve as nucleation centers for nanoparticle growth. For example, rGO linked to nanoparticles and chromophore molecules in designed multicomponent assemblies was applied to create electron transfer cascades for use in artificial photosynthesis.[30−33] Notably, while in the majority of reports rGO was considered as an electron acceptor and transporter (or "reservoir") that can enhance performance of a photocatalyst by facilitating charge separation and electron transfer from the semiconductor as well as a scaffold that increases surface area,[34] only few papers proposed rGO as a photosensitizer.[35−38]

In this work, we introduce rGO as an additional module that, along with the natural light-capturing membrane complex bR, helps to sensitize TiO_2 to visible light. Moreover, rGO provides a nanoscaffold for seamless interface between biological molecules, semiconductor particles, and platinum cocatalyst. The charge transfer from photoexcited rGO to TiO_2 was demonstrated by electron paramagnetic resonance (EPR) and transient absorption (TA) spectroscopy. The rational engineering of the nano-bio catalyst *via* introduction of rGO results in boosting photocatalytic hydrogen production performance under ambient conditions and remarkable reduction of platinum nanocatalyst content.

RESULTS AND DISCUSSION

As sketched in Figure 1a, the proposed light-driven nano-bio system employs reduced graphene oxide and membrane proton pump (bR) lattices as building blocks that serve to sensitize the TiO_2 photocatalyst to visible light, while platinum nanoparticle cocatalyst utilizes photoinduced electrons to reduce protons to hydrogen. Photoinduced holes are scavenged by methanol as a sacrificial substrate.

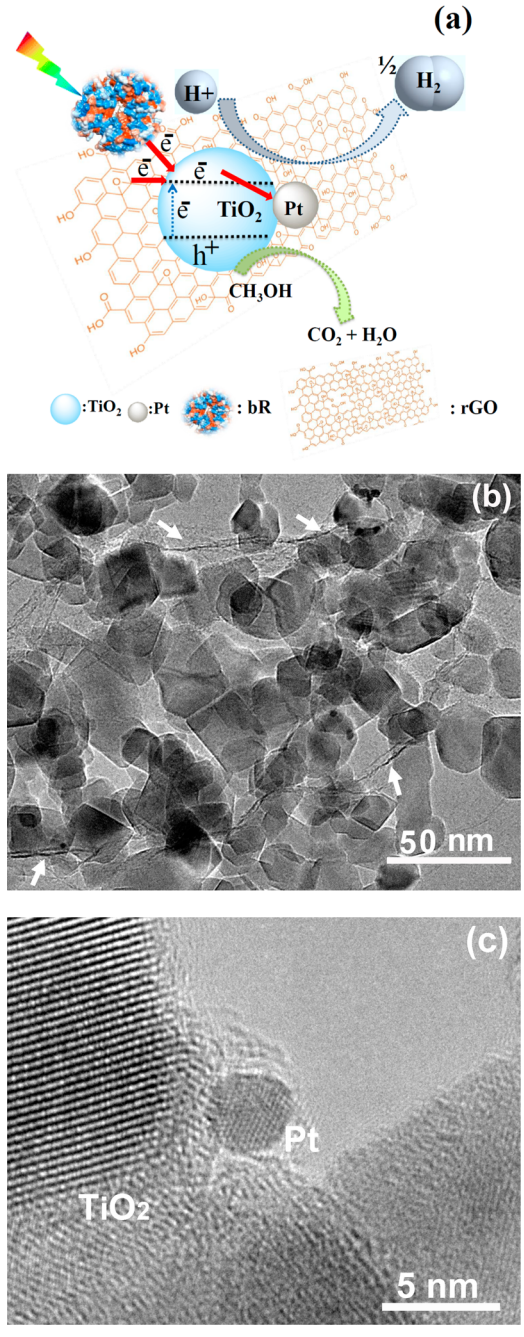

Figure 1. (a) Depiction of photocatalytic hydrogen evolution using Pt/TiO_2 interfaced with rGO and bR. (b) TEM image of the Pt/TiO_2-rGO. The white arrows point to the atomically thin rGO sheets assembled on the surface of the hybrid. (c) HRTEM image of Pt cocatalyst nanoparticles photodeposited on TiO_2.

The Pt/TiO_2-rGO system was fabricated *via* simultaneous photoreduction of GO and sodium hexachloroplatinate precursors on TiO_2 in the presence of ethanol. The total amount of graphene material used to assemble with TiO_2 was 0.5 wt %. Typical TEM images of rGO, Pt, and TiO_2 nanoparticles are shown in Figure 1b,c. TiO_2 nanoparticles (Evonik) with diameters ranging from 8 to 30 nm were dispersed on rGO uniformly. Pt metal nanoparticles with an average diameter of 3 nm grown on the semiconductor surface as well as the edges of the carbon material can be observed in the HRTEM micrograph, as shown in Figure 1b. Restored sp^2 networks of rGO and multiple available oxygen-centered surface groups allow the unified connection between the carbon material and exposed oxygen atoms at the surface of TiO_2 nanoparticles. Subsequent self-assembly of membrane−bR complexes on the surface of the Pt/TiO_2-rGO results in the Pt/TiO_2-rGO-bR visible-light-reactive nano-bio photocatalyst. It has been reported that bR can be successfully linked to carbon materials, such as carbon nanotubes, *via* noncovalent interactions or covalent tethering.[39−42] Moreover, recently, Chen and co-authors reported the fabrication of hybrid complexes based on biotinylated PM linked to avidin-functionalized graphene oxide.[43] In the current work, we employ the natural structure of the bR that allows for utilizing self-assembly, a minimalistic bioinspired time- and cost-efficient approach. Owing to availability of multiple charged groups on the cytoplasmic and extracellular sides of the PM, the biological entity readily interacts with oxygen-centered groups on the rGO. Furthermore, multiple aromatic amino acid residues (Thr, Phe, Tyr) exposed on extracellular surface (Supporting Information Figure S1) further promote well-ordered assembly of the flat 2D membrane protein on 2D rGO lattices *via* $\pi-\pi$ stacking interactions. In addition, some of the bR molecules can assemble on the exposed oxygen atoms of the anatase surface of the TiO_2 nanoparticles.[20] Accordingly, in aqueous solution, bR self-assembles on the rGO-modified TiO_2 to form a stable conjugate as observed in the UV−vis absorbance spectrum (Figure S2). The EPR data that provide further insights into the hybrid catalyst structure and interactions between biological and nanoparticle components will be discussed below.

In this work, the photocatalytic H_2 evolution driven by the Pt/TiO_2-rGO-bR nano-bio photocatalyst was evaluated under green light and white light irradiation using methanol as a sacrificial electron donor. The H_2 production activities of the Pt/TiO_2-bR were also measured for reference. The amount of Pt in Pt/TiO_2-bR and Pt/TiO_2-rGO-bR were optimized. The highest photocatalytic activities for hydrogen evolution were obtained when Pt content was 0.75 wt % in Pt/TiO_2-bR and 0.5 wt % in the carbon-material-boosted counterpart Pt/TiO_2-rGO-bR.

As shown in Figure 2a, under continuous green light (560 ± 10 nm) illumination, H_2 generation was observed with a turnover rate of approximately 298 μmol of H_2 (μmol protein)$^{-1}$ h^{-1}. The turnover rate of Pt/TiO_2-rGO-bR is higher than that of the rGO-free Pt/TiO_2-bR bio-nano catalyst (229 μmol of H_2 (μmol protein)$^{-1}$ h^{-1}). It is possible that the rGO upon excitation could inject the photogenerated electrons into the conduction band of TiO_2. However, control experiments with Pt/TiO_2 and Pt/TiO_2-rGO without bR molecules yielded lower amounts of H_2 evolved under this illumination condition. When monochromatic green light was replaced with white light illumination (λ = 350−800 nm), H_2 turnover rate of Pt/TiO_2-rGO-bR was increased by 37-fold, reaching approximately 11.24 mmol of H_2 (μmol protein)$^{-1}$ h^{-1}, which was 2 times higher than that of the Pt/TiO_2-bR nano-bio catalyst alone without rGO (5.38 mmol of H_2 (μmol protein)$^{-1}$ h^{-1}) (Figure 2b). This result clearly demonstrates that introduction of a small amount of rGO (0.5 wt %) results in improved photocatalytic performance of the nano-bio photocatalyst in hydrogen evolution and a commensurate 25% reduction of platinum content. We propose that rGO acts similarly to an organic photosynthesizer and provides additional photoexcited electrons to the conduction band of the TiO_2 particles, thus extending visible light reactivity of the semiconductor and boosting H_2 evolution over the Pt cocatalyst. Control experiments using TiO_2-bR and TiO_2-rGO-bR without Pt nanoparticles produced only minute amounts of H_2 under white light irradiation; therefore, rGO could

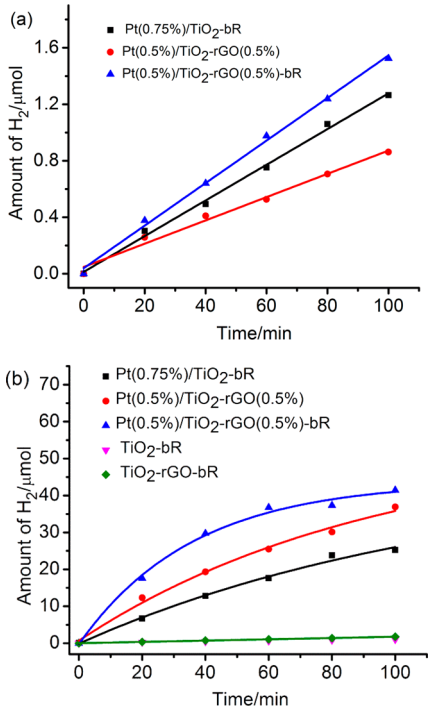

Figure 2. Photocatalytic H_2 evolution in the presence of methanol as electron donor at pH 7.0 (a) under monochromatic green light, 560 ± 10 nm (13 mW/cm^2), and (b) under white light illumination (350 nm ≤ λ ≤ 800 nm, 120 mW/cm^2).

not replace the Pt cocatalyst in the H_2 evolution process. Measurements of the photocatalytic activity of the Pt/TiO_2-rGO without bR were also carried out under white light illumination and resulted in lower H_2 evolution rate, as shown in Figure 2b, indicating that bR can enhance the H_2 evolution process. Hence, the highest performance was exhibited by the ternary nano-bio photocatalyst.

In order to confirm the collective impact of rGO and bR on the hybrid catalyst performance, photoelectrochemical measurements were carried out using the typical three-electrode system in a 0.1 M Na_2SO_4 electrolyte (pH 6.5). TiO_2 and TiO_2-rGO were also tested as references. TiO_2 nanoparticles and TiO_2-rGO were electrophoretically deposited on ITO electrodes to form a uniform film. The obtained TiO_2-rGO electrode was immersed in the bR solution overnight at room temperature, allowing the biomolecules to self-assemble on the TiO_2-rGO-modified ITO electrodes. All obtained electrodes were tested for the photocurrent generation under white light and green light illumination (560 ± 10 nm), as shown in Figure 3. The current−potential (*I*−*V*) curves of TiO_2, TiO_2-rGO, and TiO_2-rGO-bR electrodes under white light illumination are presented in Figure 3a. The photocurrent of the bare TiO_2 electrode continuously increases before reaching a steady state value of 8.4 μA/cm^2, while the current of TiO_2-rGO continues to increase before reaching a steady state value of 55 μA/cm^2 at 1.0 V *vs* Ag/AgCl. In the case of the TiO_2-rGO-bR photoelectrode, the photocurrent continues to increase before reaching a steady state value of 78 μA/cm^2, which is about 9-fold higher than that of the bare TiO_2 electrode. This result indicated that the photocurrent is predominantly coming from the photoexcited rGO which transfers the photogenerated electrons to TiO_2 nanoparticles. Comparing the current−potential curves of TiO_2-rGO and TiO2-rGO-bR presented in Figure 3a, one can observe that the so-called flat-band potential of TiO_2-rGO-bR (−0.306 V *vs* Ag/AgCl) is more anodical than that of TiO_2-rGO (−0.319 V *vs* Ag/AgCl). This anodical shift can be attributed to the protons pumped from the excited bR. TiO_2-rGO works as an n-type semiconductor electrode, and when its surface contacts an aqueous electrolyte, proton dissociation equilibrium on the surface is established for the surface hydroxide, as described below:

$$TiO_2\text{-rGO-OH} \leftrightarrow TiO_2\text{-rGO-O}^- + H^+$$

Protons released from excited bR shifts the equilibrium to the left-hand side, which leads to the anodic shift of the so-called flat-band potential, which is in agreement with work by Watanabe and co-authors.[44] Therefore, bR in our system functions as a traditional dye and proton pump.

Figure 3b,c shows the photocurrent−transient responses under white light and green light illumination,

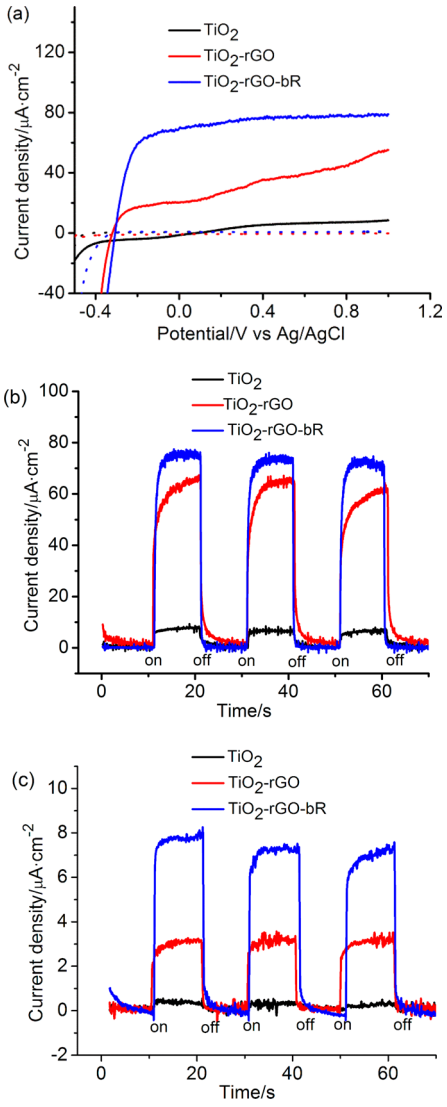

Figure 3. (a) Current−potential (*I*−*V*) curves of TiO_2, TiO_2-rGO, and TiO_2-rGO-bR electrodes under white light illumination. Dotted curves correspond to TiO_2, TiO_2-rGO, and TiO_2-rGO-bR in dark conditions. (b) Photocurrent−transient responses under white light irradiation. (c) Photocurrent−transient responses under green light irradiation. The light density of white light is 120 mW/cm^2; green light density is 13 mW/cm^2; the electrolyte is 0.1 M aqueous Na_2SO_4, pH 6.5.

respectively. In the dark, the photoelectrodes show negligible current response, while upon illumination, the photocurrent increases rapidly and reaches steady state values. Once the illumination is turned off, the photocurrent returns to the background level, and this process can be repeated many times. It follows from comparing the data presented in Figure 3b,c that the origin of the photocurrent can be mostly credited to the excitation of rGO under white polychromatic light and the excitation of bR under green light and the associated energy transfer to the TiO_2.

In order to explore the structure and electron transfer pathways within this nano-bio hybrid system, we performed electron paramagnetic resonance studies. The Pt/TiO_2-rGO nanocomposites exhibit a strong

sharp EPR signal in the dark with a line width of 1.45 G, close to that of delocalized electrons over a whole plane of the rGO, with the addition of a weak signal that corresponds to electrons delocalized at the edges/defect sites[5,45] (Figure 4a). The π-electron radical that is delocalized along the edges/defects exhibits fast spin−lattice relaxation through interaction with the adjacent π-electron system, which results in a broadening of the EPR signal.[46,47] On the other hand, in the EPR spectrum of Pt/TiO_2-rGO-bR in the dark (Figure 4a, black line), the broad signal disappears, while only the sharp signal is present. This is an indication that the bR protein predominantly adsorbs on the defect sites of rGO and "repairs" it (Figure 4a).

Under illumination with light (λ > 440 nm), the Pt/TiO_2-rGO-bR nano-bio hybrid showed a decrease in signal corresponding to delocalized electrons in the rGO, which was accompanied by the appearance of signals that correspond to the localized electrons in anatase and rutile of titania P25[48,49] (Figure 4b). These data demonstrate that rGO upon excitation with visible light injects electrons into TiO_2. Upon turning off photoexcitation, the EPR signals of the TiO_2 lattice-trapped electrons were preserved at 4.5 K, indicating that the photogenerated charges are well separated from each other, which results in their suppressed recombination (Figure S3). The EPR measurements of Pt/TiO_2-rGO nanocomposites were also carried out to confirm electron transfer from excited rGO to titania (Figure S4). The bR can also work as a light-harvesting entity capable of transferring electrons to TiO_2, which has been proven in our previous work.[20] Under white light illumination, there is probably combined input from rGO and bR, as far as contribution of the excited bR to the overall EPR spectra of illuminated Pt/TiO_2-rGO-bR hybrid can be observed (see Figure 4b inset).

To offer mechanistic insights regarding the early time carrier dynamics, transient absorption measurements were carried out on the individual and combined components. TA is capable of providing information about the time scales of charge separation in this system, which occur much more quickly than can be ascertained using EPR. Due to the presence of multiple components, charge transfer can occur through multiple pathways. However, both to simplify analysis and also because rGO, with its broad, strong optical absorption will dominate visible light absorption, all TA measurements were performed using a pump wavelength of 450 nm, which preferentially excites rGO over bR or Pt/TiO_2 (Figure S2). First, neat rGO and TiO_2-rGO with TiO_2 concentrations of 25, 50, and 75 mg mL^{-1} are compared to ascertain charge transfer from rGO to TiO_2. Figure 5a shows the visible TA spectra of rGO and TiO_2-rGO at 25 mg mL^{-1} (TA spectra for 50 and 75 mg mL^{-1} are in Supporting Information, Figure S5). Upon 450 nm excitation, rGO produces a bleach from ~475 to 675 nm and a photoinduced absorption (PA) from ~675 to 800 nm. TiO_2-rGO

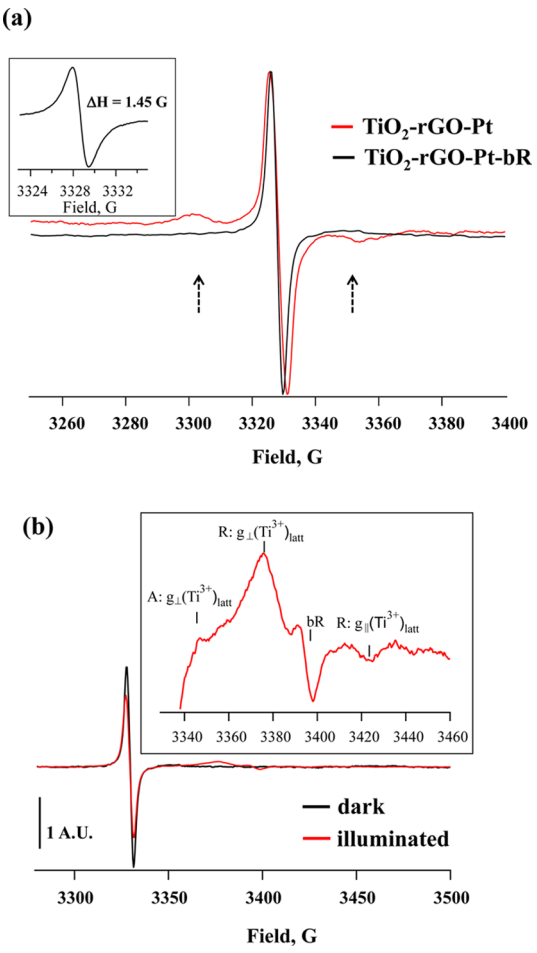

Figure 4. (a) X-band EPR spectra of Pt/TiO_2-rGO (red line) and Pt/TiO_2-rGO-bR (black line) measured in the dark at 4.5 K; power = 2.08 mW, modulation amplitude = 8 G. Inset: EPR spectrum of Pt/TiO_2-rGO in the dark at 4.5 K; power = 2.08 mW, modulation amplitude = 1 G. (b) X-band EPR spectra of Pt/TiO_2-rGO-bR at 4. 5K in the dark (black line) and under illumination; λ > 440 nm (red line), power = 2.08 mW, modulation amplitude = 8 G. Inset: difference between spectra under illumination and dark, showing formation of signals that correspond to the lattice-trapped electrons in TiO_2: anatase (A) and rutile (R).

exhibits similar spectral features; however, the intensity of the bleach and PA decay more rapidly. The decay of the bleach signal was further investigated by analyzing the dynamics at 520 nm, the wavelength at which the bleach signal is the largest. The decay traces at 520 nm were fitted with an exponential function: $y = A^*\exp(-x/\tau) + y_0$, where τ is the decay lifetime and A is the corresponding amplitude. The average decay lifetime was consistently faster in the TiO_2-rGO system as compared to neat rGO (Figure 5b). Specifically, neat rGO decayed with a time constant of 6.09 ± 0.50 ps, whereas Pt/TiO_2-rGO decayed with a lifetime of 3.32 ± 0.26 ps. This result demonstrates charge transfer from rGO to TiO_2 and supports a conclusion from EPR studies. Next bR and rGO-bR were examined to investigate charge transfer within this system. The TA measurements of rGO-bR show rGO bleach signals that decay faster than neat rGO. Analysis of the dynamics at 520 nm produces a decay constant of 3.41 ± 0.20 ps for

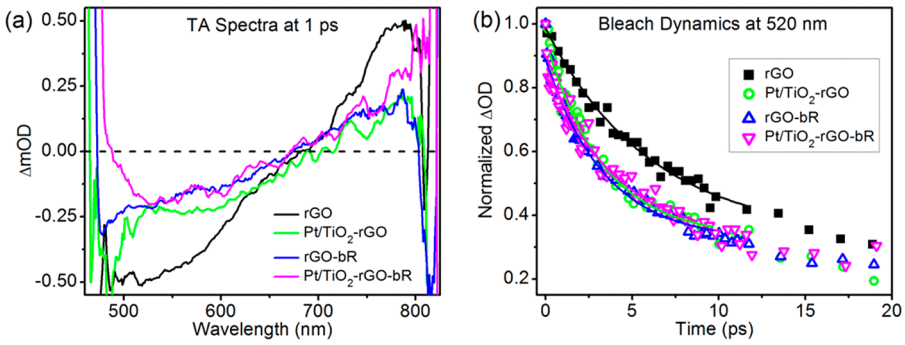

Figure 5. Ultrafast TA measurements of rGO, TiO_2-rGO, rGO-bR, and TiO_2-rGO-bR. (a) TA spectra at 1 ps delay time exhibits two major spectral features: a bleach from ~475 to 675 nm and a photoinduced absorption from ~675 to 800 nm. (b) Bleach dynamics at 520 nm show that TiO_2-rGO, rGO-bR, and TiO_2-rGO-bR decay more rapidly than neat rGO, suggestive of charge transfer from rGO to the other components.

rGO-bR, faster than that for neat rGO (Figure 5b). This result suggests that charge transfer can also occur from rGO to bR, which was not established from EPR studies. A similar analysis of the dynamics of TiO_2-rGO-bR (TiO_2 concentration was 25 mg mL^{-1}) at 520 nm produces a decay constant of 3.49 ± 0.54 ps (Figure 5b). The decay lifetimes for TiO_2-rGO, rGO-bR, and TiO_2-rGO-bR are equivalent within error, and as a result, the specific order of charge transfer (*i.e.*, rGO transfers an electron directly to Pt/TiO_2, or rGO transfers an electron to bR, which then transfers the charge to Pt/TiO_2 on a 1 ps time scale, as previously established[20]) cannot be distinguished through TA measurements. Ultimately, however, the order of charge transfer is not influential because previous work established that for the TiO_2-bR complex, charge transfer occurs from bR to TiO_2.[20] Thus, even if rGO transfers an electron to bR, reduced bR will subsequently transfer the charge to TiO_2.

CONCLUSIONS

Herein, we report the successful interfacing of Pt/TiO_2 hybrid nanoparticles with two building modules—an avant-garde 2D graphene material rGO and "pre-historical" 2D biomaterial membrane proton pump bR in synergistically integrated catalytic system for solar hydrogen production. Both the rGO and bR materials possess excellent properties, including structural simplicity and intrinsic robustness at a variety of environmental conditions. Moreover, they can readily self-assemble with Pt/TiO_2 nanoparticles without additional chemical coupling steps to form a stable and functional hierarchical photocatalytic system. The resulting Pt/TiO_2-rGO-bR nano-bio device is able to produce H_2 at a turnover rate of 298 μmol of H_2 (μmol protein)$^{-1}$ h^{-1} under monochromatic green light and 11.24 mmol of H_2 (μmol protein)$^{-1}$ h^{-1} under white light illumination at room temperature and neutral pH. Furthermore, an introduction of the carbon material allows for a reduction in the platinum cocatalyst content by 25%. Introduction of rGO and bR into the photocatalyst results in approximately 9-fold increase in photocurrent density compared to the unmodified TiO_2 electrode. This increase in photocurrent is associated with collective charge injections from both rGO and bR molecules to TiO_2 nanoparticles. In addition, the honeycomb lattice of rGO promotes seamless interactions between biological and inorganic modules as well as between distinct TiO_2 nanoclusters in this ternary nano-bio photocatalyst. The EPR and TA measurements proved that charge transfer occurs from the excited rGO and bR molecules to the TiO_2. This study demonstrates that reduced graphene oxide can be utilized as a multifunctional module for the rational engineering and fabrication of efficient, stable, and environmentally benign photocatalysts for solar energy conversion.

MATERIALS AND METHODS

Graphene oxide was from Sigma-Aldrich; TiO_2 (Evonik Industries, P-25) containing anatase and rutile in 80:20 ratio with a surface area of ~55 m^2g^{-1} was used as a main support. Bacteriorhodopsin from *Halobacterium salinarum* was obtained from Sigma-Aldrich and used without further purification. Active bR protein concentrations were determined spectrophotometrically using the molar extinction coefficient of 62 700 M^{-1} cm^{-1} at λ_{max} = 568 nm. Sodium hexachloroplatinate, ethanol, methanol, hydrochloric acid, sodium sulfate, acetone, iodine were obtained from Sigma-Aldrich. Deionized (DI) ultrapure water (18 MΩ·cm^{-1}) was used for solution preparation.

Photocatalyst Synthesis and Assembly. Pt/TiO_2-rGO hybrid particles were prepared *via* simultaneous photoreduction of GO and sodium hexachloroplatinate precursors on TiO_2 (P25). A typical GO reduction along with platinum particle deposition was carried out in a 8 mL vial containing aqueous suspension of TiO_2 (3 mg/mL) in the presence of 1 mL of ethanol, 22.5 μL of 2 mg/mL graphene oxide, and 0.043 mg/mL sodium hexachloroplatinate. The slurry pH was adjusted to ~3 using 1 M HCl. The suspension was stirred thoroughly and purged with high-purity N_2 for 30 min to remove dissolved oxygen. After purging, the slurry was irradiated in white light ($\lambda \geq 350$ nm) using a 200 W high-pressure Xe lamp (PerkinElmer Optoelectronics) for 30 min. A 10 cm water filter was used to cutoff IR radiation. After irradiation, the particles were centrifuged and washed with DI water three times. The final Pt/TiO_2-rGO photocatalyst particles were stored in DI water before use. As it was determined by inductively coupled plasma–atomic emission spectroscopy analyses, the typical Pt loading was 0.5 wt %. The rGO concentration was calculated to be ~0.5 wt %.

To prepare the nano-bio catalyst, bR solution (0.0039 μmol) was added to 1 mL of the Pt/TiO_2-rGO (3 mg/mL) photocatalyst particle slurry in DI water. The mixture was agitated overnight to enable maximum bR absorption on the particles' surface. The optical characterizations of the TiO_2, TiO_2-rGO, and TiO_2-rGO-bR were performed using a Varian UV−vis spectrophotometer UV-50.

Hydrogen Evolution Measurements. The freshly prepared bR-modified Pt/TiO_2-rGO particles were transferred to a 1 mL water/methanol (4:1 volume) solution reaction vessel sealed tightly with a rubber septum. The mixture was degassed with high-purity N_2 for 30 min. High-pressure Xe lamp (200 W) equipped with a 10 cm IR water filter and a band-pass filter (560 ± 10 nm) was used as the light source. Green light intensity of 13 mW/cm^2 and white light intensity of 120 mW/cm^2 were determined by a light intensity meter (NOVAII laser power/energy monitor). The amount of photogenerated H_2 was detected and quantified with an Agilent 7890A gas chromatograph (GC) equipped with a thermal conductivity detector and HP PLOT Molesieve 5 Å column, which was held isothermally at 40 °C. Pure N_2 (99.999%+) was used as a carrier gas at a flow rate of 3.5 mL min^{-1}. At the interval time, 20 μL aliquots of the gas sample from the headspace of the reaction vessel were collected and analyzed by the GC system.

Preparation of TiO_2, TiO_2-rGO, and TiO_2-rGO-bR Photoelectrodes. TiO_2, TiO_2-rGO, and TiO_2-rGO-bR photoelectrodes were prepared by electrophoretic deposition on an ITO electrode (area 1 cm^2) using Ti sheets as a counter electrode. The typical electrophoretic deposition was performed in acetone solution (50 mL) containing TiO_2 or TiO_2-rGO particles (50 mg) and iodine (10 mg). ITO and Ti sheets were dipped into the solution 1 cm apart, and then 120 V bias was applied between them for 1 min using a potentiostat (Agilent E3612A). The film was then sintered at 250 °C in Ar gas for 20 min. The obtained TiO_2-rGO electrode was modified with bR (0.0018 μmol/mL) with overnight immersing in the dark and then rinsed with DI water before measurement.

Photoelectrochemical Measurements. The photoelectrochemical properties were investigated by a three-electrode system with TiO_2, TiO_2-rGO, or TiO_2-rGO-bR as working electrodes, saturated Ag/AgCl as a reference electrode, and platinum wire as a counter electrode. The electrolyte was 0.1 M Na_2SO_4 at pH 6.5, and before measurement, the electrolyte was purged with pure N_2 (99.999%+) for 30 min to remove dissolved oxygen. High-pressure Xe lamp (200 W) equipped with a 10 cm IR water filter and a band-pass filter (560 ± 10 nm) was used as the light source. The light densities of white light and green light were set to 120 and 13 mW/cm^2. A potentiostat (BAS-100W) was employed to measure illuminated linear current−potential curve at a scan rate of 20 mV/s. Transient photocurrent curves of different photoelectrodes were carried out at potentiostatic conditions (500 mV *vs* Ag/AgCl electrode) under white light and green light irradiation.

EPR. Continuous-wave EPR experiments were carried out using a Bruker ELEXSYS E580 spectrometer operating in the X-band (9.4 GHz) mode and equipped with an Oxford CF935 helium flow cryostat with an ITC-5025 temperature controller. The **g** tensors were calibrated for homogeneity and accuracy by comparison to a coal standard, **g** = 2.00285 ± 0.00005. The receiver gain and number of scans were adjusted to every spectrum of a particular sample to enable comparisons at a reasonable signal-to-noise ratio. For the studies of charge transfer pathways, samples were deaerated by bubbling with N_2 for *ca.* 30 min, frozen at liquid He temperature, and illuminated in the EPR cavity using a 300 W Xe lamp (PerkinElmer) with 440 nm long-pass and water as IR cutoff filters.

Transient Absorption Measurements. Transient absorption measurements were performed using a 2 kHz, 35 fs amplified Ti:sapphire laser. A portion of the 800 nm laser fundamental was mechanically delayed and focused into a sapphire plate to produce a broad-band white light probe. Pump pulses at 450 nm (fluence 75 μJ/cm^2) were produced using an optical parametric amplifier. Samples were measured under ambient conditions.

Conflict of Interest: The authors declare no competing financial interest.

Acknowledgment. This work was performed at the Center for Nanoscale Materials, a U.S. Department of Energy, Office of Science, Office of Basic Energy Sciences User Facility under Contract No. DE-AC02-06CH11357.

Supporting Information Available: Includes structure of PM and bR (Figure S1), UV−vis spectra (Figure S2), EPR spectra of Pt/TiO_2-rGO-bR at 4.5 K in the dark, under illumination (λ > 440 nm), 5 min in dark after illumination (Figure S3), EPR spectra Pt/TiO_2-rGO at 4.5 K in the dark and under illumination (Figure S4), TA spectra of (a) neat rGO and TiO_2-rGO at TiO_2 concentrations of (b) 25, (c) 50, and (d) 75 mg mL^{-1} (Figure S5), typical GC trace for H_2 evolution (Figure S6) and TON based on bR and rGO. This material is available free of charge *via* the Internet at http://pubs.acs.org.

REFERENCES AND NOTES

1. Lewis, N. S. Toward Cost-Effective Solar Energy Use. *Science* **2007**, *315*, 798–801.
2. Maeda, K.; Teramura, K.; Lu, D. L.; Takata, T.; Saito, N.; Inoue, Y.; Domen, K. Photocatalyst Releasing Hydrogen from Water. *Nature* **2006**, *440*, 295.
3. Yoon, T. P.; Ischay, M. A.; Du, J. N. Visible Light Photocatalysis as a Greener Approach to Photochemical Synthesis. *Nat. Chem.* **2010**, *2*, 527–532.
4. Rau, S.; Schäfer, B.; Gleich, D.; Anders, E.; Rudolph, M.; Friedrich, M.; Görls, H.; Henry, W. G.; Vos, J. A Supramolecular Photocatalyst for the Production of Hydrogen and the Selective Hydrogenation of Tolane. *Angew. Chem., Int. Ed.* **2006**, *45*, 6215–6218.
5. Wang, P.; Minegishi, T.; Ma, G. J.; Takanabe, K.; Satou, Y.; Maekawa, S.; Kobori, Y.; Kubota, J.; Domen, K. Photoelectrochemical Conversion of Toluene to Methylcyclohexane as an Organic Hydride by Cu_2ZnSnS_4-Based Photoelectrode. *J. Am. Chem. Soc.* **2012**, *134*, 2469–2472.
6. Fujishima, A.; Honda, K. Electrochemical Photolysis of Water at a Semiconductor Electrode. *Nature* **1972**, *238*, 37–38.
7. Chen, X. B.; Liu, L.; Yu, P. Y.; Mao, S. S. Increasing Solar Absorption for Photocatalysis with Black Hydrogenated Titanium Dioxide Nanocrystals. *Science* **2011**, *331*, 746–750.
8. Gao, F. F.; Wang, Y.; Shi, D.; Zhang, J.; Wang, M. K.; Jing, X. Y.; Humphry-Baker, R.; Wang, P.; Zakeeruddin, S. M.; Grätzel, M. Enhance the Optical Absorptivity of Nanocrystalline TiO_2 Film with High Molar Extinction Coefficient Ruthenium Sensitizers for High Performance Dye-Sensitized Solar Cells. *J. Am. Chem. Soc.* **2008**, *130*, 10720–10728.
9. Chen, X.; Shen, S.; Guo, L.; Mao, S. S. Semiconductor-Based Photocatalytic Hydrogen Generation. *Chem. Rev.* **2010**, *110*, 6503–6570.
10. Tong, H.; Ouyang, S.; Bi, Y.; Umezawa, N.; Oshikiri, M.; Ye, J. Nano-photocatalytic Materials: Possibilities and Challenges. *Adv. Mater.* **2012**, *24*, 229–251.
11. Utschig, L. M.; Silver, S. C.; Mulfort, K. L.; Tiede, D. M. Nature-Driven Photochemistry for Catalytic Solar Hydrogen Production: A Photosystem I-Transition Metal Catalyst Hybrid. *J. Am. Chem. Soc.* **2011**, *133*, 16334–16337.
12. Utschig, L. M.; Dimitrijevic, N. M.; Poluektov, O. G.; Chemerisov, S. D.; Mulfort, K. L.; Tiede, D. M. Photocatalytic Hydrogen Production from Noncovalent Biohybrid Photosystem I/Pt Nanoparticle Complexes. *J. Phys. Chem. Lett.* **2011**, *2*, 236–241.
13. Reisner, E.; Powell, D. J.; Cavazza, C.; Fontecilla-Camps, J. C.; Armstrong, F. A. Visbile Light-Driven H_2 Production by Hydrogenases Attached to Dye-Sensitized TiO_2 Nanoparticles. *J. Am. Chem. Soc.* **2009**, *131*, 18457–18466.
14. Goldet, G.; Wait, A. F.; Cracknell, J. A.; Vincent, K. A.; Ludwig, M.; Lenz, O.; Friedrich, B.; Armstrong, F. A. Hydrogen Production under Aerobic Conditions by Membrane-Bound Hydrogenases from Ralstonia Species. *J. Am. Chem. Soc.* **2008**, *130*, 11106–11113.
15. Roth, L. E.; Nguyen, J. C.; Tezcan, F. A. ATP- and Iron-Protein-Independent Activation of Nitrogenase Catalysis by Light. *J. Am. Chem. Soc.* **2010**, *132*, 13672–13674.
16. Roth, L. E.; Tezcan, F. A. Light-Driven Uncoupling of Nitrogenase Catalysis from ATP Hydrolysis. *ChemCatChem* **2011**, *3*, 1549–1555.

17. Yuhas, B. D.; Smeigh, A. L.; Douvalis, A. P.; Wasielewski, M. R.; Kanatzidis, M. G. Photocatalytic Hydrogen Evolution from FeMoS-Based Biomimetic Chalcogels. *J. Am. Chem. Soc.* **2012**, *134*, 10353–10356.
18. Bora, D. K.; Rozhkova, E. A.; Schrantz, K.; Wyss, P. P.; Braun, A.; Graule, T.; Constable, E. C. Functionalization of Nanostructured Hematite Thin-Film Electrodes with the Light-Harvesting Membrane Protein C-Phycocyanin Yields an Enhanced Photocurrent. *Adv. Funct. Mater.* **2012**, *22*, 490–502.
19. Shimura, K.; Yoshida, H. Heterogeneous Photocatalystic Hydrogen Production from Water and Biomass Derivatives. *Energy Environ. Sci.* **2011**, *4*, 2467–2481.
20. Balasubramanian, S.; Wang, P.; Schaller, R. D.; Rajh, T.; Rozhkova, E. A. High-Performance Bioassisted Nanophotocatalyst for Hydrogen Production. *Nano Lett.* **2013**, *13*, 3365–3371.
21. Allam, N. K.; Yen, C.-W.; Near, R. D.; El-Sayed, M. A. Bacteriorhodopsin/TiO_2 Nanotube Arrays Hybrid System for Enhanced Photoelectrochemical Water Splitting. *Energy Environ. Sci.* **2011**, *4*, 2909–2914.
22. Hamp, N. Bacteriorhodopsin as a Photochromic Retinal Protein for Optical Memories. *Chem. Rev.* **2000**, *100*, 1755–1776.
23. Xie, G.; Zhang, K.; Guo, B.; Liu, Q.; Fang, L.; Gong, J. R. Graphene-Based Materials for Hydrogen Generation from Light-Driven Water Splitting. *Adv. Mater.* **2013**, *25*, 3820–3839.
24. Zhang, N.; Zhang, Y.; Xu, Y.-J. Recent Progress on Graphene-Based Photocatalysts: Current Status and Future Perspectives. *Nanoscale* **2012**, *4*, 5792–5813.
25. Xiang, Q.; Yu, J. G.; Jaroniec, M. Graphene-Based Semiconductor Photocatalysts. *Chem. Soc. Rev.* **2012**, *41*, 782–796.
26. Yeh, T.-F.; Cihlar, J.; Chang, C.-Y.; Cheng, C.; Teng, H. Roles of Graphene Oxide in Photocatalytic Water Splitting. *Mater. Today* **2013**, *16*, 78–84.
27. Novoselov, K. S.; Geim, A. K.; Morozov, S. V.; Jiang, D.; Zhang, Y.; Dubonos, S. V.; Grigorieva, I. V.; Firsov, A. A. Electric Field Effect in Atomically Thin Carbon Films. *Science* **2004**, *306*, 666–669.
28. Liang, Y. T.; Vijayan, B. K.; Gray, K. A.; Hersam, M. C. Minimizing Graphene Defects Enhances Titania Nanocomposite-Based Photocatalytic Reduction of CO_2 for Improved Solar Fuel Production. *Nano Lett.* **2011**, *11*, 2865–2870.
29. Akhavan, O. Graphene Nanomesh by ZnO Nanorod Photocatalysts. *ACS Nano* **2010**, *4*, 4174–4180.
30. Tu, W. G.; Zhou, Y.; Liu, Q.; Tian, Z. P.; Gao, J.; Chen, X. Y.; Zhang, H. T.; Liu, J. G.; Zou, Z. G. Robust Hollow Spheres Consisting of Alternating Titania Nanosheets and Graphene Nanosheets with High Photocatalytic Activity for CO_2 Conversion into Renewable Fuels. *Adv. Funct. Mater.* **2012**, *22*, 1215–1221.
31. Zhang, J.; Yu, J. G.; Jaroniec, M.; Gong, J. R. Noble Metal-Free Reduced Graphene Oxide-$Zn_xCd_{1-x}S$ Nanocomposite with Enhanced Solar Photocatalytic H_2-Production Performance. *Nano Lett.* **2012**, *12*, 4584–4589.
32. Yadav, R. K.; Baeg, J. O.; Oh, G. H.; Park, N. J.; Kong, K. J.; Kim, J.; Hwang, D. W.; Biswas, S. K. A Photocatalyst−Enzyme Coupled Artificial Photosynthesis System for Solar Energy in Production of Formic Acid from CO_2. *J. Am. Chem. Soc.* **2012**, *134*, 11455–11461.
33. Hayashi, H.; Lightcap, I. V.; Tsujimoto, M.; Takano, M.; Umeyama, T.; Kamat, P. V.; Imahori, H. Electron Transfer Cascade by Organic/Inorganic Ternary Composites of Porphyrin, Zinc Oxide Nanoparticles, and Reduced Graphene Oxide on a Tin Oxide Electrode That Exhibits Efficient Photocurrent Generation. *J. Am. Chem. Soc.* **2011**, *133*, 7684–7687.
34. Yang, N. L.; Liu, Y. Y.; Wen, H.; Tang, Z. Y.; Zhao, H. J.; Li, Y. L.; Wang, D. Photocatalytic Properties of Graphdiyne and Graphene Modified TiO_2: From Theory to Experiment. *ACS Nano* **2013**, *2*, 1504–1512.
35. Fan, W. Q.; Lai, Q. H.; Zhang, Q. H.; Wang, Y. Nanocomposites of TiO_2 and Reduced Graphene Oxide as Efficient Photocatalysts for Hydrogen Evolution. *J. Phys. Chem. C* **2011**, *115*, 10694–10701.
36. Bai, X. J.; Wang, L.; Zhu, Y. F. Visible Photocatalytic Activity Enhancement of $ZnWO_4$ by Graphene Hybridization. *ACS Catal.* **2012**, *2*, 2769–2778.
37. Bai, X. J.; Wang, L.; Zong, R. L.; Lv, Y. H.; Sun, Y. Q.; Zhu, Y. F. Performance Enhancement of ZnO Photocatalyst *via* Synergic Effect of Surface Oxygen Defect and Graphene Hybridization. *Langmuir* **2013**, *29*, 3097–3105.
38. Zhang, Y.; Zhang, N.; Tang, Z. R.; Xu, Y. J. Graphene Transforms Wide Band Gap ZnS to a Visible Light Photocatalyst the New Role of Graphene as a Macromolecular Photosensitizer. *ACS Nano* **2012**, *6*, 9777–9789.
39. El Hadj, K.; Bertoncini, P.; Chauvet, O. pH-Sensitive Photoinduced Energy Transfer from Bacteriorhodopsin to Single-Walled Carbon Nanotubes in SWNT-bR Hybrids. *ACS Nano* **2013**, *7*, 8743–8752.
40. Ingrosso, C.; Bianco, G. V.; Corricelli, M.; Corcelli, A.; Lobasso, S.; Bruno, G.; Agostiano, A.; Striccoli, M.; Curri, M. L. Hybrid Charge Transfer Complexes Based on Archaeal Glycolipids Wrapping Single Walled Carbon Nanotubes. *Chem. Commun.* **2013**, *49*, 6941–6943.
41. Ingrosso, C.; Bianco, G. V.; Lopalco, P.; Tamborra, M.; Curri, M. L.; Corcelli, A.; Bruno, G.; Agostiano, A.; Siciliano, P.; Striccoli, M. Surface Chemical Functionalization of Single Walled Carbon Nanotubes with a Bacteriorhodopsin Mutant. *Nanoscale* **2012**, *4*, 6434–6441.
42. Bertoncini, P.; Chauvet, O. Conformational Structural Changes of Bacteriorhodopsin Adsorbed onto Single-Walled Carbon Nanotubes. *J. Phys. Chem. B* **2010**, *114*, 4345–4350.
43. Chen, H.-M.; Lin, C.-J.; Jheng, K.-R.; Kosasih, A.; Chang, J.-Y. Effect of Graphene Oxide on Affinity-Immobilization of Purple Membranes on Solid Supports. *Colloids Surf., B* **2014**, *116*, 482–488.
44. Saga, Y.; Watanabe, T.; Koyama, K.; Miyasaka, T. Mechanism of Photocurrent Generation from Bacteriorhodopsin on Gold Electrodes. *J. Phys. Chem. B* **1999**, *103*, 234–238.
45. Su, C.; Acik, M.; Takai, K.; Lu, J.; Hao, S.-J.; Zheng, Y.; Wu, P.; Bao, Q.; Enoki, T.; Chabal, Y. J.; Loh, K. P. Probing the Catalytic Activity of Porous Grapheme Oxide and the Origin of This Behavior. *Nat. Commun.* **2012**, *3*, 1298.
46. Pham, C. V.; Krueger, M.; Eck, M.; Weber, S.; Erdem, E. Comparative Electron Paramagnetic Resonance Investigation of Reduced Graphene Oxide and Carbon Nanotubes with Different Chemical Functionalities for Quantum Dot Attachment. *Appl. Phys. Lett.* **2014**, *104*, 132102.
47. Rao, S. S.; Stesmans, A.; Wang, Y.; Chen, Y. Direct ESR Evidence for Magnetic Behavior of Graphite Oxide. *Physica E* **2012**, *44*, 1036–1039.
48. Li, G.; Dimitrijevic, N. M.; Chen, L.; Nichols, J. M.; Rajh, T.; Gray, K. A. The Important Role of Tetrahedral Ti^{4+} Sites in the Phase Transformation and Photocatalytic Activity of TiO_2 Nanocomposites. *J. Am. Chem. Soc.* **2008**, *130*, 5402–5403.
49. Grabstanowicz, L. R.; Gao, S. M.; Li, T.; Rickard, R. M.; Rajh, T.; Liu, D. J.; Xu, T. Facile Oxidative Conversion of TiH_2 to High-Concentration Ti^{3+}-Self-Doped Rutile TiO_2 with Visible-Light Photoactivity. *Inorg. Chem.* **2013**, *52*, 3884–3890.